Preventing HO-TriggeredCovalent Cross-Linking Enables All-Aqueous Processable and RecoverableFunctionalized Polythiophene-Based Cellulose

CHEMISTRY OF MATERIALS

Open Access

pubs.acs.org/cm

Article

Preventing H_2O_2-Triggered Covalent Cross-Linking Enables All-Aqueous Processable and Recoverable Functionalized Polythiophene-Based Cellulose Coatings

Johanna Heimonen,* Cecilia Bruschi, Asaminew Y. Shimolo, Marle E. J. Vleugels, Lukas Marcos Celada, Sozan Darabi, Viktor Gueskine, Daniel Primetzhofer, Christian Müller, Bence Fehér, Peter Olsén, and Renee Kroon*

Cite This: https://doi.org/10.1021/acs.chemmater.6c01062

Read Online

ACCESS | Metrics & More | Article Recommendations | Supporting Information

ABSTRACT: The transition to sustainable electronics requires electroactive materials that are processable in green solvents, operationally stable, and recyclable or recoverable at their end of life. This work explores recoverable electroactive cellulose coatings using a carboxylate-functionalized polar polythiophene (PCAT-K). PCAT-K is water-processable and can be reversibly fixated onto cellulose threads by modulation of the secondary interactions via acid−base chemistry, showing promise for circular material use. To obtain electrically conducting PCAT-K-cellulose threads, acid-mediated oxygen doping of the PCAT-K with *p*-toluenesulfonic acid was explored but led to undesired covalent cross-linking and loss of solubility and recoverability. Through spectroscopic and electrochemical analyses, it is shown that the covalent cross-linking originates from hydrogen peroxide generation during the doping process, which further reacts with PCAT to form hydroxyl radicals. To suppress radical formation, potassium iodide is introduced as a benign additive that catalytically decomposes hydrogen peroxide, preventing covalent cross-linking while maintaining electrical conductivity and recoverability. While the additive can negatively affect cellulose substrates at long doping times, this strategy allows for stable, conductive, and removable electroactive coatings on cellulose threads using water as the sole solvent. This study highlights a more reliable synthetic route to the water-processable conjugated polymer PCAT-K and suggests a mechanistic origin of acid-mediated oxygen doping-induced covalent cross-linking with a practical strategy to overcome it.

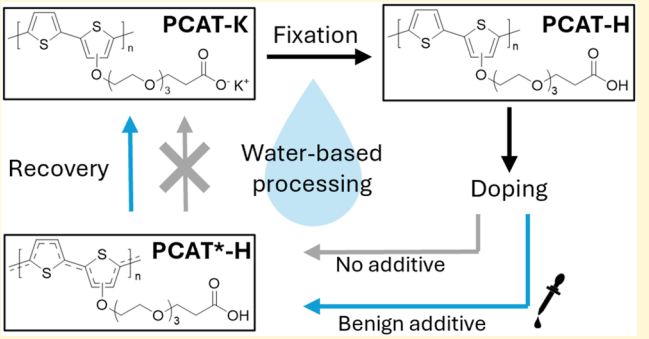

INTRODUCTION

The transition to a greener society requires a comprehensive approach regarding the design and development of new materials.[1] To aid in the development of more sustainable materials, the 'Safe and Sustainable by Design' (SSbD) framework has been initiated by the European Union, where green material development is considered directly at the design stage. The SSbD framework includes replacement or minimization of harmful substances, as well as reducing the impact on health, climate, and the environment during the whole supply chain.[2] This strategy can involve creating materials that can be entirely or partially biobased, material designs that allow for aqueous processing schemes as well as circular designs that facilitate separation of materials at their end-of-life for recovery or reuse.

Conjugated polymers (CPs) stand out as a class of organic materials because of their physicochemical and optoelectronic properties, which can be carefully tuned by strategic chemical design.[3−8] Owing to their weak mechanical properties, CPs are most often used in combination with a glass or plastic supporting substrate. More recently, CPs have been explored in the form of composites and coatings that combine biobased reinforcement with cellulose with the electronic or photonic properties of CPs, as a way to introduce new functions into wood- or cellulose-based materials.[9−12] Efficient recycling of hybrid materials often relies on the separation of the components into separate waste streams, which is complicated by the lack of chemical design motifs for recycling, recovery, or removal in state-of-the-art CPs. While the fully organic nature of such composite materials would, in principle, allow for incineration at their end of life, the embedded energy of CPs is

Received: April 10, 2026
Revised: June 26, 2026
Accepted: June 30, 2026

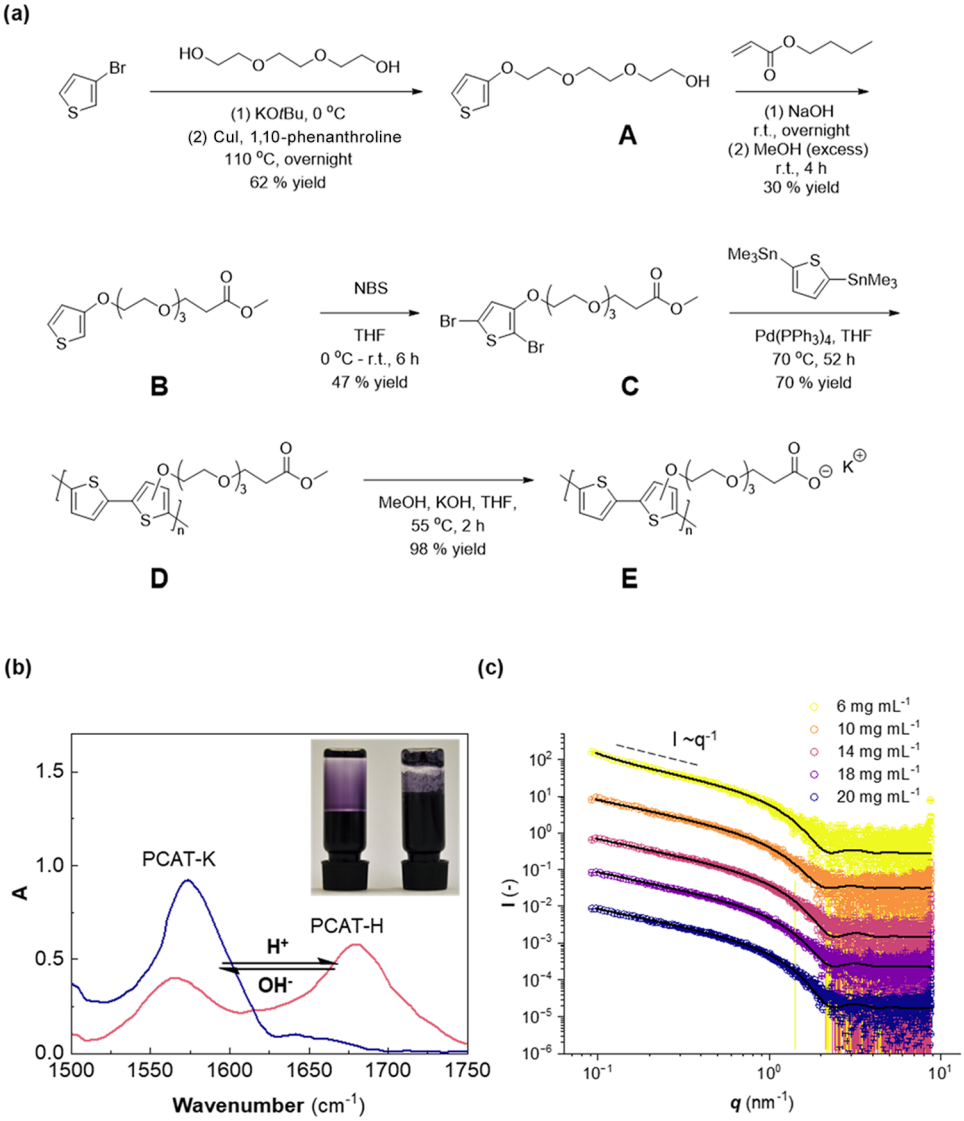

Figure 1. (a) Synthetic scheme for PCAT-K via PCAT-Me. (b) FTIR of pH-switchable protonation of the PCAT carboxylate group with exposure to citric acid (10 mg mL^{-1}, see Figure S10 for full spectra), inset shows the polymer solubility in DI water for PCAT-K (left) and PCAT-H (right). c) SAXS scattering profiles of PCAT-K at different concentrations (symbols) and corresponding rigid cylinder model fits (black line) in H_2O. The power law scaling of $I \sim q^{-1}$ at low q is indicated by the dashed line, which is indicative for the formation of elongated structures. Data is shifted vertically for clarity.

high due to the many synthesis steps needed to produce them,[13] warranting exploration of chemical or physical removal, recovery or recycling.

Several chemical design strategies have been explored to enable chemical recycling of CPs.[14] Most chemically recyclable CPs utilize a combination of reversible imine-based chemistry and solvent-based extraction for removal and recovery of the degradation products.[15−18] Imine linkages can be incorporated into CPs, which permit acid-triggered degradation into dialdehyde- and diamine-functionalized monomers, which can be collected via organic solvent extraction for reuse. The use of imine chemistry does, however, preclude the use of water-based processing strategies and water-containing cellulose as this will hydrolyze the imine linkages. Another strategy that has been explored is oxidative cleavage of triple-bond containing CPs, utilizing oxygen or other reactive oxygen species (ROS). With this strategy, degradation products have been collected and repurposed, though synthesis of the parent polymer has not yet been achieved.[19,20]

Chemical removal, recovery or recycling strategies have not yet been explored for water-processable CPs, such as the ubiquitous poly(2,3-dihydrothieno-1,4-dioxin):poly(styrenesulfonate) (PEDOT:PSS). Despite its excellent electrical properties and stability with water-processability, the presence of sulfonate counterions in PEDOT:PSS requires postprocessing covalent cross-linking with (3-glycidyloxypropyl)trimethoxysilane (GOPS) to obtain an electroactive material with good adhesive and cohesive properties in aqueous environment,[21] which prevents chemical recycling by dissolution. Recently, the Reichmanis group has explored several carboxylate-functionalized polythiophenes, where chemical fixation was achieved through protonation with a strong organic acid.[22−24] This design motif has the potential for benign and reversible cross-linking and could facilitate the removal of CPs from a substrate at the end of life.

https://doi.org/10.1021/acs.chemmater.6c01062
Chem. Mater. XXXX, XXX, XXX−XXX

An additional advantage of using strong organic acids for fixation is the possibility of attaining a desired long-term stability, previously demonstrated to yield electroactive materials stable for up to half a year.[25]

Thus, it is still a challenge to unify water-processability of CPs with sufficient electrical stability and benign reversible cross-linking chemistry that allows for material recovery. In this work, we develop the reversible cross-linking of the carboxylate-functionalized polar polythiophene PCAT-K[26] when using this material as a recoverable electroactive coating on cellulose threads. PCAT-K can be reversibly fixed to and released from a cellulose substrate through pH modulation of its water solubility using citric acid and potassium hydroxide (KOH). However, during acid-mediated oxygen doping with p-toluenesulfonic acid (p-TsOH), this reversibility is lost due to covalent cross-linking. We show that hydrogen peroxide (H_2O_2) is formed during acid-mediated oxygen doping. The produced H_2O_2 undergoes a subsequent redox reaction with PCAT, forming hydroxyl radicals, which leads to covalent cross-linking. To address this undesired cross-linking, a targeted synthetic strategy was implemented using potassium iodide (KI). Here, KI suppresses covalent cross-linking by decomposing hydrogen peroxide (H_2O_2) into H_2O and O_2, enabling PCAT to function as a removable electroactive coating on both glass substrates and cellulose threads fibers without compromising electrical conductivity or long-term stability.

RESULTS AND DISCUSSION

Material Selection

For this work, we chose to use a water-soluble regiorandom carboxylate-functionalized polar polythiophene—PCAT-K with a low ionization energy(IE) of −4.65 eV.[26] A low IE is advantageous since it facilitates low operating voltages in case of organic transistors as well as facile p-type doping for applications that require electrically conducting materials.[27,28] PCAT-K's potassium carboxylate functionalization of the oligoethylene glycol side chain offers several features: (1) the carboxylate group offers good solubility in water, (2) the relatively low p*K*a of carboxylates (typically p*K*a 2−5) facilitates protonation of the carboxylate group via exposure to dilute acid solutions, thereby changing solvation behavior and allowing for physical cross-linking through secondary interactions after drying,[7] and (3) this physical cross-linking is largely retained at neutral pH and can be reversed through exposure to alkaline solutions. Depending on the p*K*a of the acid it can work as a cross-linking agent or a cross-linking dopant to obtain a semiconducting or fully conducting material.[29] Cellulose is a suitable and easily available sustainable substrate for PCAT-K due to its mechanical strength, compatibility with water and availability of many sites for both hydrophobic interactions and hydrogen bonding.[30] After aqueous processing of PCAT-K onto cellulose threads and protonation, the combined reduced water-solubility and secondary interactions can be expected to increase both the adhesion between the electroactive coating and a cellulose substrate as well as the cohesive strength of the electroactive coating.[31] The PCAT-K and cellulose can then be separated on demand via aqueous alkaline treatment.

Optimized Synthesis of PCAT-K

Following a previously reported synthetic route[26] (Scheme S1), deprotection of the *tert*-butyl ester prepolymer PCAT-*t*Bu was done with trifluoroacetic acid (TFA) in formic acid as the only viable mixture to dissolve the resulting carboxylic acid-functionalized CP (designated PCAT-H). Treating PCAT-H with a KOH solution yielded the desired water-soluble polyanionic potassium salt form, PCAT-K. The conversion from PCAT-*t*Bu to PCAT-K was shown to result in batch-to-batch variations of PCAT-K's water solubility, likely due to the use of the strong acid TFA during the *tert*-butyl deprotection step (Table S1). To improve synthetic reliability, the synthetic route was altered to a final deprotection of a methyl ester using milder conditions (KOH, 10 w%, aq), as reported in Figure 1a.

The monomer (**C**) was synthesized in 3 steps (see SI for detailed synthetic procedure). In the first step, a neat Ullman etherification reaction was performed, yielding the glycolated-thiophene intermediate **A** in 62% yield. *Oxa*-Michael addition of butyl acrylate to compound **A** resulted in the addition of a protected acid-functionality. Butyl acrylate was chosen as the Michael acceptor since methyl acrylate resulted in very low yields due to radical self-polymerization. Butyl acrylate instead allows for a one-pot transesterification to a methyl ester, (Compound **B**, 30% yield) and enables easy removal of the transesterification byproduct.[32] The methyl ester also facilitates easy and benign deprotection of the final polymer. The dibrominated monomer (**C**) was obtained in 45% yield by bromination with *N*-bromosuccinimide (NBS) and subsequently polymerized via Stille cross-coupling to yield the prepolymer PCAT-Me (**D**). The final water-soluble polymer PCAT-K (**E**) was obtained by deprotection through hydrolysis of the PCAT-Me prepolymer with aqueous KOH (10 w%) for 2 h. NMR analysis of intermediates, monomer and polymer are reported in Figures S1−S8.

Due to the availability of PCAT-K derived from PCAT-*t*Bu, we chose from here-on to perform our studies with this material. The molecular weight of the PCAT-*t*Bu polymer was determined by gel permeation chromatography (GPC), yielding values of $M_n \sim 12$ kg mol^{-1} (∼27 repeat units) and a Đ of 3.8 (Values for PCAT-Me can be found in Table S2). In an attempt to analyze the protonation reaction in solution, we performed titration experiments on the deprotected monomer and the polymer PCAT-K. For the carboxylate-functionalized monomer we determined a single equivalence point around pH 7, while we determined 2 equivalence points for PCAT-K (pH ∼8 and 4.5, Figure S9) likely due to a combination of carboxylate protonation, pH-induced conformational changes and backbone doping due to the use of a strong acid. Upon exposure to a weak acid solution (citric acid, 10 mg mL^{-1}, pH ∼2.2), the carboxylate groups on PCAT-K will be protonated, altering the solubility of the polymer (Figure 1b).[33]

To establish whether water solutions of PCAT-K exist as true solutions as opposed to large particle dispersions, we performed synchrotron small-angle X-ray scattering (SAXS) on aqueous solutions of PCAT-K. Power law analysis at low *q* revealed a slope of −1, indicative for the formation of cylindrical structures in solution. The presence of cylindrical particles was further supported by least-squares fitting of the experimental data using a rigid cylinder model with a circular cross-section (Figure 1c). Interestingly, the fitting parameters revealed a clear trend as a function of PCAT-K concentration. With increasing concentration, the cylinder length decreased markedly; between the 6 mg mL^{-1} and 20 mg mL^{-1} samples, the cylinder length decreased by approximately 1 order of magnitude (from ∼400 nm to ∼60 nm, Table S3), whereas the cross-sectional radius remained essentially unchanged (∼1.6

https://doi.org/10.1021/acs.chemmater.6c01062
Chem. Mater. XXXX, XXX, XXX−XXX

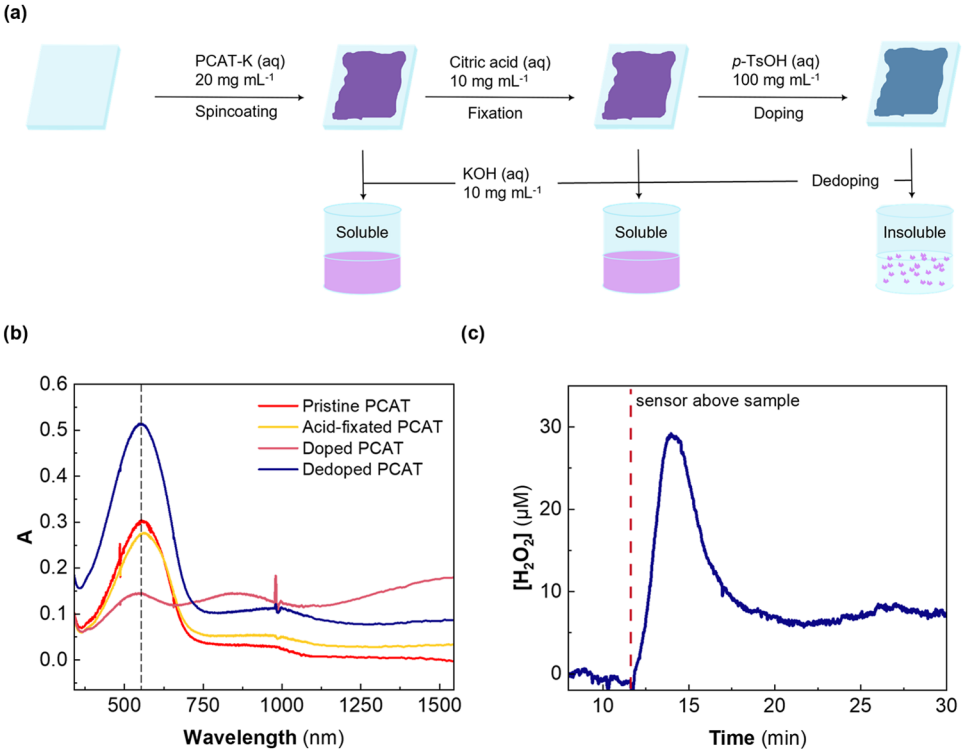

Figure 2. (a) Doping procedure for PCAT thin films. (b) UV−vis spectra of a single thin film of pristine PCAT-K, PCAT-H after fixation, treatment with *p*-TsOH and then treatment with KOH. (c) Amperometric sensor measurements of dropcast μm-thick films of PCAT-*t*Bu (80 μL, 20 mg mL^{-1} solution) on glass in oxygen-sparged *p*-TsOH (aq, 250 mg mL^{-1}).

nm). It is also worth noting that the most dilute sample (6 mg mL^{-1}) exhibited slightly elevated scattering intensity at low q, indicative of weak interparticle aggregation. To account for this contribution, a power-law term was included in the fitting model. These results indicate that more dilute PCAT-K exists as elongated chains that can more easily assemble into longer cylindrical particles, while at higher concentrations the PCAT-K chains are less prone to assemble. We conclude that PCAT-K exists as a fine dispersion of small, elongated particles rather than as a coarse dispersion comprising microscopic aggregates.

Doping Studies

To study PCAT-K as an electroactive coating, we developed the manufacturing scheme presented in Figure 2a. First, PCAT-K is coated on a clean glass slide, which is subsequently dried and fixated by dipping the slide into a citric acid solution, chosen due to its benign nature, yielding the semiconducting form of the material. The semiconducting coating could then be separated from the glass substrate via aqueous alkaline treatment.

We chose to treat PCAT with *p*-TsOH to obtain the fully conducting form of PCAT-H, as similar polar polythiophenes treated with sulfonic acids display a high electrical conductivity with a long shelf life.[25] We postulated that the doping process is similar to acid-mediated oxygen doping described by Mammone et al. for polyacetylene, which involves molecular oxygen as the electron acceptor, features the peroxide ion O_2^{2-} and H_2O_2 as intermediates and yields water as a byproduct.[34] For efficient acid-mediated oxygen doping to occur the sample should be in contact with air. Therefore, two doping procedures were explored (see SI for doping procedure development): dip-and-dry (Doping procedure 1) or soaking (Doping procedure 2). We optimized the dopant concentration (c_{doping}) and time (t_{doping}) and found that Doping procedure 1 at c_{doping} = 100 mg mL^{-1} *p*-TsOH (aq) and t_{doping} = 2 h resulted in the highest doping level of PCAT (Figure S11).

As we attempted to recover doped PCAT from the glass substrate by treatment with KOH (aq, 10 mg mL^{-1}, 60 °C) we observed that the polymer would detach as insoluble purple flakes instead of dissolving (aq, 10 mg mL^{-1}, 60 °C. See Figure S12), which precluded solution-based analyses of the observed effect. This contrasted with our observations of PCAT that was only fixated with citric acid (a weak acid), which would readily redissolve in aqueous KOH solutions. To investigate under which conditions solubility was affected and if loss of solubility could be prevented, we varied the experimental conditions such as light, oxygen, water, type of acid, additives and recovery solvent for doping and recovery (Table S4). All initial variations of doping and recovery protocols proved unsuccessful, indicative of cross-linking. As glycolated polythiophenes are commonly used within the organic electronics community, we decided to thoroughly investigate the cause of the structural changes to gain a deeper understanding of the active processes when these CPs are exposed to air and acidic water and to find a way of preventing the negative effects.

Origin of Chemical Cross-Linking

We considered several explanations for the change in solubility behavior: the presence of polarons, cleavage of the side chains, chemical degradation of the backbone and covalent cross-linking. We investigated the integrity of the conjugated backbone by comparing the UV−vis spectrum of thin films of PCAT-H before and after doping via exposure to *p*-TsOH and after dedoping by treatment with KOH. The UV−vis spectrum of PCAT-H before and after treatment with *p*-TsOH

https://doi.org/10.1021/acs.chemmater.6c01062
Chem. Mater. XXXX, XXX, XXX−XXX

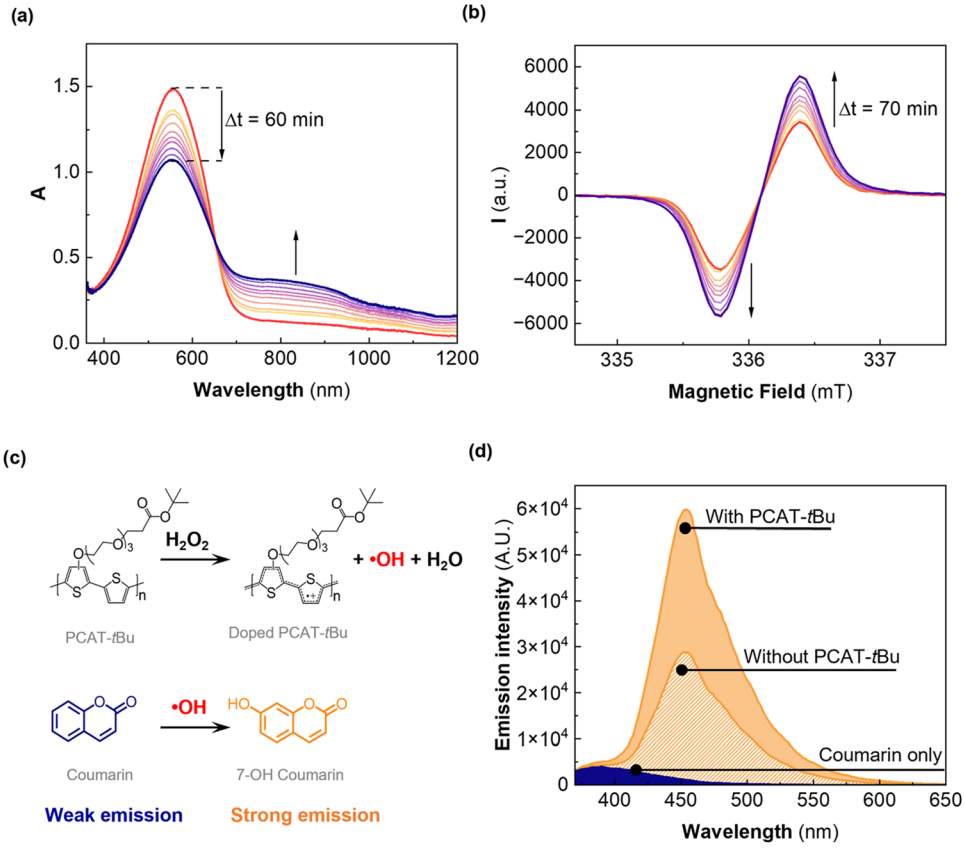

Figure 3. (a) Absorption spectra evolution of a PCAT-K solution (aq, 0.05 mg mL^{-1}) after addition of H_2O_2 (0.02 M) under light and air atmosphere. (b) Evolution of the EPR spectra from an aqueous PCAT-K (3 mg mL^{-1}) solution (blue line) after addition of H_2O_2 (0.1 M) in light and under air atmosphere recorded over 70 min. The intensity of the polaron peak is increasing after the addition of H_2O_2, which confirms oxidation of PCAT-K by H_2O_2. (c) Principle of the $^{\bullet}OH$ radical detection. The proposed reaction starts with the polymer reacting with H_2O_2 producing $^{\bullet}OH$ radicals. The radical is then scavenged by coumarin, a poorly emitting compound, which is partially converted to 7-OH coumarin, the only fluorescent product. (d) Emission spectra of coumarin experiments, average of three measurements.

are identical, whereas severe backbone degradation would manifest itself as a blueshift in the optical absorption. We note that treating the films with KOH results in rapid dedoping of the films, evidenced by the recovery of the optical absorption of the neutral polymer, which also rules out that the change in solubility originates from the presence of polarons on the polymer backbone (Figure 2b).

To assess the integrity of the side chains we analyzed the FT-IR spectrum of PCAT-K that was subjected to a doping/dedoping cycle, using the nonbrominated CAT-monomer as a reference for the peaks (Figure S13). Both the C−H stretch ($\nu \sim 3030-2770$ cm^{-1}) and the C−O stretch ($\nu \sim 1100$ cm^{-1}) do not appear to change in intensity, which means that the concentration of side chains has not markedly changed due to the doping process. Therefore, we can also rule out significant side chain cleavage as the reason for the change in solubility and we argue that chemical cross-linking is the most likely cause.

We hypothesized, following recent suggestions,[34,35] that H_2O_2 (and potentially derived ROS) is formed during acid-mediated oxygen doping of PCAT-H. Based on previous studies on CP-mediated oxygen reduction reaction (ORR) to H_2O_2,[36−38] we considered two possible pathways for the formation of H_2O_2. Both pathways start with a one-electron reduction of molecular oxygen (O_2) by PCAT-H (P^0) that yields first $O_2^{\bullet-}$ and upon reaction with H^+ the hydroperoxyl radical ($HOO^{\bullet}$) at pH < 4.88, in a continuous process according to eq 1.

$$P^0 + O_2 + H^+ + TSO^- \leftrightharpoons P^{+\bullet}(TSO^-) + HOO^{\bullet} \quad (1)$$

The first pathway (eq 2) would have $HOO^{\bullet}$ migrate to a nearby oxidizable site on the PCAT-H backbone where a second one-electron reduction of the $HOO^{\bullet}$ results in H_2O_2.

$$P^0 + HOO^{\bullet} + H^+ + TSO^- \leftrightharpoons P^{+\bullet}(TSO^-) + H_2O_2 \quad (2)$$

The second pathway does not involve further redox doping of the PCAT-H (eq 3). Instead, two hydroperoxyl radicals undergo a disproportionation process, which is kinetically pH-dependent, thereby forming H_2O_2 and O_2.[38]

$$2HOO^{\bullet} \leftrightharpoons H_2O_2 + O_2 \quad (3)$$

To investigate whether H_2O_2 is formed during the acid-mediated oxygen doping of PCAT, we monitored the doping reaction with amperometric sensor measurements of drop-casted PCAT-*t*Bu (80 μL, 20 mg mL^{-1} solution) on glass in oxygen bubbled *p*-TsOH solution (250 mg mL^{-1}). Handling of material for the H_2O_2 production tests was performed with glass to avoid unnecessary contact with metals. These measurements confirm that H_2O_2 is produced during doping, as shown in Figure 2c. H_2O_2 is produced at the polymer:-electrolyte interface, it is not detected away from the film, and its concentration decreases over time. We explain the latter

https://doi.org/10.1021/acs.chemmater.6c01062
Chem. Mater. XXXX, XXX, XXX−XXX

observation by the H_2O_2 production slowing down over time as the PCAT is depleted of electrons, combined with the H_2O_2 slowly dissipating into the whole volume of the solution. Additionally, we exposed drop-casted films of PCAT-*t*Bu to dilute H_2O_2 (0.001 M for 1 h) and observed the same irreversible change in solubility and formation of flakes when doping the polymer, showing that H_2O_2 was not only produced but likely the cause of the insolubility.

While H_2O_2 is a strong oxidant, it does not have the capability to result in hydrogen atom transfer (HAT), which would be needed to initiate cross-linking reactions. Instead, cleavage of H_2O_2 would be needed to produce more active ROS, that could cause HAT. The two most obvious sources for the observed covalent cross-linking are either the hydroperoxyl radical or the hydroxyl radical. Considering the bond dissociation energy (BDE) of an ether C−H bond (∼92 kcal mol^{-1}), the most likely source of covalent cross-linking through HAT is the hydroxyl radical, with water forming as the product of the reaction (BDE ∼ 119 kcal mol^{-1}).[39] Hydroperoxide radicals are less reactive (BDE of ∼ 88 kcal mol^{-1}), forming H_2O_2 as the product. In our case, H_2O_2 could be converted into the much more reactive hydroxyl radical via Fenton-like reactions,[40,41] catalyzed by the presence of residual iron or copper from the synthesis.[42] Hydroxyl radicals could then abstract a hydrogen atom from the side chain, forming a carbon radical that ultimately results in a covalent cross-link. To investigate the composition and residual metal content in PCAT-K, in particular iron and copper, Rutherford Backscattering Spectrometry (RBS) and Particle Induced X-ray Emission (PIXE) were performed. RBS confirms the expected K:S ratio in PCAT-K, while RBS and PIXE further indicate that trace amounts of iron and surprisingly chromium are present in PCAT-K, likely from handling the samples with stainless steel implements (See Figure S14 and Table S5 and SI for further discussion). Inductively Coupled Plasma Mass Spectrometry (ICP-MS) was performed to verify the amounts of copper and iron and indicates only ppm-level quantities of each metal. Palladium, while present in larger quantities in the polymer, does not work as an active catalyst for Fenton-type reactions.[43] Based on these results, we conclude that ppm-level iron and copper impurities in PCAT-K are likely not the cause of covalent cross-linking, and that generation of ROS should proceed through a different mechanism.

Our final hypothesis for the origin of the cross-linking was that the PCAT, due to its low ionization energy, could reduce H_2O_2 to the $^{\bullet}OH$ radical and OH^- (H_2O under acidic conditions), akin to the Vitamin C/H_2O_2 initiator system[44] (eq 4)

$$H_2O_2 + e^- \rightarrow {}^{\bullet}OH + OH^- (H_2O \text{ under acidic conditions}) \quad (4)$$

This reaction would then compete with the first electron reduction of O_2 to $HOO^{\bullet}$, which is sluggish due to its low reduction potential ($E^0 = -0.07$ V vs SHE).

To study whether PCAT would undergo such a redox reaction with H_2O_2, we mixed PCAT-K with H_2O_2 in water solution and recorded the evolution of the optical absorption over time (Figure 3a). Slow oxidation of PCAT-K occurs after addition of H_2O_2, evidenced by the decrease of the parent polymer peak (λ_{max} = 557 nm) and the appearance of a polaron peak in the 700−1100 nm range. We observe that the doping process accelerated with a larger amount of H_2O_2 (Figure S15). The same spectral evolution was obtained repeating the experiment in the dark and under inert atmosphere indicating that light and oxygen are not involved in this reaction (Figure S16). We note the appearance of an isosbestic point at 655 nm, which suggests the presence of a chemical equilibrium and excludes the possibility of significant polymer backbone degradation.

Similar results were obtained with electron paramagnetic resonance (EPR) spectroscopy. The EPR spectrum of a PCAT-K water solution kept under air atmosphere presented a signal with a g-factor 2.013 and no hyperfine splitting, which can be attributed to the well-known formation of polarons induced by oxidation of p-type polymers (Figure S17).[45] The EPR intensity of the PCAT-K polaron peak was monitored for 1 h. During this time, the peak intensity only slightly decreased, probably related to the sample warming up from room temperature to the higher cavity temperature (T_{cavity} = 36 °C), which favors a dedoping process. In contrast, after addition of H_2O_2 to a PCAT-K solution monitored over the course of 70 min, the polaron peak increased in intensity (Figure 3b). The analysis performed in the dark gave similar results to those obtained when the solution was exposed to light (Figure S18). The EPR results corroborate the UV−vis spectroscopy results and lead us to the conclusion that a redox reaction occurs between the PCAT-K polymer and H_2O_2.

As stated in (eq 4), the predicted product from the reaction between PCAT and H_2O_2 is the $^{\bullet}OH$ radical. To probe for the $^{\bullet}OH$ radical, we performed a series of reactions with coumarin, a known selective probe for hydroxyl radicals.[46,47] Coumarin is a weakly emitting compound and while its reaction with $^{\bullet}OH$ radicals yield several products, only 7-hydroxy-coumarin (7-OH) is fluorescent and can be used for detection (Figure 3c). Since PCAT-K is significantly absorbing in the same wavelength range where 7-OH is emitting (λ = 400−600 nm), a polymer solution cannot be used for detection of potential $^{\bullet}OH$ radicals. Instead, we choose to use films of PCAT-*t*Bu, which is energetically similar to PCAT-K without risk of delamination from the glass substrate as PCAT-H films. Accordingly, a 1 mL solution of H_2O_2 (0.1 M) and coumarin (0.05 mM) was applied on top of a spin-coated film of PCAT-*t*Bu and left for 20 h. in the dark. Pristine glass slides were treated using the same conditions and used as a reference. The emission spectrum of 7-OH in the collected solutions was recorded at an excitation wavelength of 332 nm (Figure 3d). The solution in contact with the PCAT-tBu film shows an almost two times higher emission compared to the reference. We explain the observation of 7-OH in the blank by HO−OH bond instability in H_2O_2, which can cleave homolytically due to bond polarization during interaction with hydrogen bond donors or acceptors, in combination with the long reaction time. We underline that, in the presence of PCAT-*t*Bu, the amount of $^{\bullet}OH$ radicals produced is underestimated due to its competing reaction with PCAT-*t*Bu. We also like to point out that, while the material properties (water uptake, ion mobility, oxygen diffusion, morphology) likely differ between PCAT-*t*Bu and PCAT-K/H, this would only affect the reaction kinetics but not the reaction mechanism itself. These results support the idea of hydroxyl radical production by the reaction between H_2O_2 and PCAT, thus enabling undesired covalent cross-linking.

https://doi.org/10.1021/acs.chemmater.6c01062
Chem. Mater. XXXX, XXX, XXX−XXX

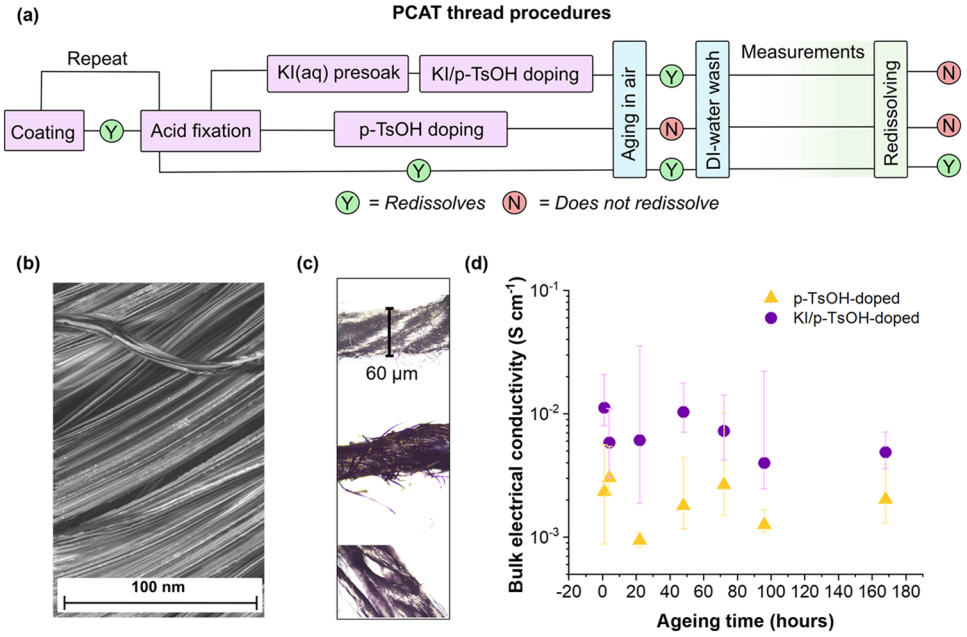

Figure 4. (a) Procedure for manufacturing PCAT threads including solubility at different stages. (b) SEM image of *p*-TsOH/KI doped threads. (c) Microscopy images of pristine threads (top), double coated threads (middle) and threads after redissolving the PCAT (bottom). (d) Bulk electrical conductivity of double coated threads (Ø ~ 60 μm) doped with and without KI-addition over 170 h, with highest and lowest values for each time point indicated by the graph bars.

Cross-Linking Remediation

Since acid-mediated oxygen doping of PCAT-K inevitably resulted in chemical cross-linking due to the redox reaction with H_2O_2, we set out to develop a strategy to prevent the formation of reactive radicals from H_2O_2. We found inspiration in the well-known elephant toothpaste experiment, where the breakdown of H_2O_2 into H_2O and O_2 is catalyzed by the addition of potassium iodide (KI) according to (eq 5).

$$2H_2O_2 \xrightarrow{KI(cat)} 2H_2O + O_2 \quad (5)$$

The KI catalyzed breakdown of H_2O_2 is very rapid and should be able to decompose the H_2O_2 and avoid the formation of hydroxyl radicals. KI is also cheap, available, metal-free, benign and can be molecularly dissolved in water allowing easy ingression into the polymer and removal after the doping process. A new doping solution, consisting of *p*-TsOH (100 mg mL^{-1}) and KI (0.5 equiv) was formulated and used to dope spin-coated films of PCAT following the dip-and-dry protocol. We observed the formation of molecular iodine (I_2) in the doping solution after approximately 1 h, as KI will break down over time in acidic solutions.[48] I_2 formation was enhanced by increased concentration of KI and/or p-TsOH (Table S6). Molecular iodine can dope CPs but the presence of an excess of acid dopant together with the instability of I_2-doping in air should make this effect negligible at the concentrations used for doping.[49] However, lower KI concentration (0.25 equiv) was insufficient to quickly break down H_2O_2 and the solubility issues reappeared. We explain the need for relatively high concentrations of KI (50 mg mL^{-1}) with the formation (and presence) of H_2O_2 close to the PCAT backbone. This strategy allowed us to successfully recover PCAT-K after doping without inducing covalent cross-linking, as confirmed by UV−vis-NIR and Dynamic light scattering (Figure S19).

Electroactive Cellulose Thread

We chose to investigate the reversible coating of cellulose threads, a model substrate of relevance for wearable electronics.[11,50−53] To obtain electroactive cellulose threads, we have developed the following manufacturing scheme (Figure 4a) (See SI for full doping procedure). Commercial Lyocell multifilament yarn (consisting mainly of ref 54,33) was separated into threads with an average diameter of 63 μm (Table S7). The cellulose threads were immersed into a solution of PCAT-K (aq, 20 mg mL^{-1}), dried in air and the polymer was subsequently fixated by dipping the coated threads into a citric acid solution. The coating step can be repeated to increase the thickness of the polymer coating, making it more durable and filling in potential gaps in the coating that form as the polymer contracts during the acid fixation step. We chose to use single or double-coated threads to minimize the use of material while ensuring a sufficiently covering layer of polymer was deposited on each thread. For threads that were to be doped with *p*-TsOH/KI, a presoak in KI (aq) followed by drying was performed to ensure a high concentration of KI was present in the coating to enable fast breakdown of H_2O_2.

To analyze the PCAT-cellulose coating, we first employed scanning electron microscopy (SEM). SEM imaging indicates that the PCAT-coating on the cellulose threads is very thin and appears to be uniform (Figure 4b). Visual inspection confirms that the PCAT is present, as a clear color change from white to dark purple is observed (Figure 4c). Energy-dispersive X-ray spectroscopy (EDX) imaging was done to further study the presence of PCAT on the cellulose thread. After coating, EDX confirmed an increase in the amount of sulfur from 0% mass for pristine cellulose threads (Figure S20) to ~6.9 mass % for PCAT-coated threads. After the acid-fixation step the sulfur content decreases to ~4.7 mass % (Figures S21−S22). The doped form of the polymer was obtained by exposing the coated cellulose thread to a *p*-TsOH (aq) solution, with or

https://doi.org/10.1021/acs.chemmater.6c01062
Chem. Mater. XXXX, XXX, XXX−XXX

without addition of 0.5 mol equiv KI, before drying the thread and acid-mediated oxygen doping in air. Near-complete removal of the coating with KOH (aq, 10 mg mL^{-1}) for either *p*-TsOH or *p*-TsOH/KI doped threads could be achieved, with sulfur contents of 0.5 mass % (*p*-TsOH doped) and 0.23 mass % (*p*-TsOH/KI doped) (Figures S23–S24). Akin to our observations for the thin films, PCAT coatings on threads doped with *p*-TsOH do not redissolve in hot base, the coating will instead detach as flakes from the cellulose substrate. In contrast, the PCAT cellulose coatings that were doped with *p*-TsOH/KI retain their ability to be redissolved, showing that the addition of KI to the doping solution is an effective strategy to prevent covalent cross-linking (Figure S25).

Next, we wanted to determine the bulk electrical conductivity of the produced threads. Before measuring the electrical resistivity of the doped threads, the threads were washed in DI water and dried to remove any remaining acid or KI to avoid ionic conduction and hygroscopic effects affecting the measurements. Resistance of the doped threads was measured in two-point configuration by mounting 1 cm threads on plastic using carbon paste (Figure S26). Carbon paste was chosen due to its good interaction with the polymer coating,[55] while silver paste, silver ink and carbon fiber were tried but resulted in large variations of the recorded electrical resistivities. Threads doped with *p*-TsOH/KI show a slightly higher bulk electrical conductivity ($\sigma_{avg,t0} = 1.1 \times 10^{-2}$ S cm^{-1}) than those doped with only *p*-TsOH ($\sigma_{avg,t0} = 2.3 \times 10^{-3}$ S cm^{-1}). All doped PCAT:cellulose threads show a slight decrease in their bulk electrical conductivity over time when threads are stored at ambient temperature in air for 170 h (Figure 4d).

Finally, we noted that Lyocell threads treated with *p*-TsOH/KI lose their structural integrity during the aging process, where the cellulose became brittle after 72 h of aging. The brittleness could be almost entirely reversed by washing in DI water, but removal of PCAT from the cellulose substrate via hot aqueous base was then no longer possible. It was, however, possible to redissolve PCAT doped for the same amount of time but not washed with DI water, indicating that this was likely an effect of the cellulose substrate. Cellulose reference samples (Table S8), showed that KI, especially in combination with acid, was the cause of structural degradation of the substrate. Initial X-ray diffraction results indicate that the cellulose II crystallite structure is affected by the doping procedure, potentially trapping the PCAT-side chains in the cellulose matrix (Figure S27).[56] This detrimental substrate effect poses a limitation to applying PCAT as a removable cellulose coating when using acid-mediated oxygen doping with long doping times. Further investigations are needed to establish the correlation between doping time, substrate degradation, and trapping of PCAT but was not performed within the scope of this work.

CONCLUSIONS

In summary, we demonstrate a strategy for stable, conductive, and removable electroactive coatings on cellulose threads using water as the sole solvent. We developed a new, more reliable route for the synthesis of the carboxylate-functionalized polar polythiophene PCAT-K. We have shown that H_2O_2 is produced during acid-mediated oxygen doping of PCAT with *p*-toluenesulfonic acid. The produced H_2O_2 reacts with the polymer, resulting in p-doping and leading to the formation of hydroxyl radicals that are the likely cause of covalent cross-linking of PCAT. We propose that changes in solubility behavior can serve as a simple initial probe to determine whether aqueous device operation has altered the material properties of conjugated polymers. We demonstrate that covalent cross-linking can be prevented by addition of KI added to the dopant solution, while not interfering with the doping process. PCAT can be used as an electroactive coating on cellulose threads and allows fixation and removal through modulation of pH, if the doping time is kept moderate to avoid the substrate being affected by the treatment. Further research is needed to establish the structural position of the unwanted covalent cross-linking, alternative strategies for suppressing these cross-links and to determine if the removed PCAT-coating material can be recycled after use.

EXPERIMENTAL SECTION

Chemicals

All reagents and solvents were purchased from Sigma-Aldrich and used as received, except for 2,5-bis(trimethylstannyl)thiophene which was recrystallized from methanol prior to use.Commercial white Lyocell Yarn was obtained from Vinterverkstaden.se.

Synthetic Methods

Compound A: 2-(2-(2-(Thiophen-3-yloxy)ethoxy)ethoxy)-ethan-1-ol. *Ullman Aryl Ether Synthesis.* To a 100 mL two-necked round-bottom flask containing triethylene glycol (7.10 g, 47.0 mmol, 7.0 equiv), potassium *tert*-butoxide (1.03 g, 9.2 mmol, 1.5 equiv) was added in portions under nitrogen atmosphere at 0 °C and stirred for 20 min, followed by 10 min at room temperature giving a light-yellow clear solution. Copper iodide (0.06 g, 0.3 mmol, 0.05 equiv) and 1,10-phenanthroline (0.22 g, 1.2 mmol, 0.1 equiv) were added slowly and stirred for 1 h at 50 °C during which the light-yellow solution was converted to light brown and upon heating to dark brown. 3-bromothiphene (1.0 g, 6.1 mmol, 1.0 equiv) was added dropwise and the reaction mixture was heated to 110 °C for 36 h. Reaction progress was monitored by thin layer chromatography in diethyl ether. The crude mixture was transferred to a separatory funnel containing 30 mL dichloromethane and extracted with 30 mL of water, the resulting emulsion was broken by addition of 30 mL brine. The organic layer was separated, dried over anhydrous magnesium sulfate, filtered through cellulose filter paper and concentrated on rotary evaporator. The product was purified on a silica gel column with 95:5 diethyl ether:methanol as the eluent. Fractions containing the product were combined, the solvent evaporated, yielding 0.88 g (62%) of a light-yellow oil. The ^{1}H NMR and ^{13}C NMR are depicted in Figures S1 and S2, respectively. (^{1}H NMR (500 MHz, $CDCl_3$) δ 7.16 (dd, J = 5.3, 3.1 Hz, 1H), 6.78 (dd, J = 5.2, 1.5 Hz, 1H), 6.26 (dd, J = 3.2, 1.6 Hz, 1H), 4.12 (dd, J = 5.7, 3.8 Hz, 2H), 3.89–3.79 (m, 2H), 3.70 (dddd, J = 14.0, 8.3, 6.0, 4.3 Hz, 7H), 3.64–3.58 (m, 2H)). (^{13}C NMR (126 MHz, $CDCl_3$) δ 157.8, 125.0, 119.9, 97.9, 72.8, 71.1, 70.7, 70.0, 69.8, 62.1)

Compound B: Methyl 4-(2-(2-(2-(thiophen-3-yloxy)ethoxy)-ethoxy)ethoxy)propanoate. *Oxa-Michael Addition and Trans-esterification.* A 50 mL two-necked round-bottom flask was charged with compound A (1 g, 5.6 mmol, 1 equiv) and sodium hydroxide (0.11 mg, 2.8 mmol, 0.5 equiv) and stirred under nitrogen for 30 min. Then, *n*-butyl acrylate (4.4 g, 11.2 mmol, 2 equiv) was added dropwise while the reaction was shielded from light with aluminum foil and stirred at room temperature overnight. An excess of methanol (15 mL) was added directly to the reaction mixture and stirred at reflux for 4 h. The vessel was cooled to RT, and the content was transferred to separatory funnel containing dichloromethane (30 mL) and the phases were separated. Deionized H_2O (40 mL) was added, and the aqueous phase was extracted with dichloromethane (2 × 20 mL). The combined organic phase was dried over anhydrous magnesium sulfate, filtered through cellulose filter paper and concentrated on rotary evaporator. The product was purified on a

https://doi.org/10.1021/acs.chemmater.6c01062
Chem. Mater. XXXX, XXX, XXX–XXX

silica gel column and eluted with 80:20 petroleum ether:acetone. The solvent was removed by evaporation, and the product was dried in vacuo overnight and yielded 0.81 g (46%) as a light-yellow oil. The ^{1}H NMR and ^{13}C NMR are depicted in Figures S3 and S4, respectively. (^{1}H NMR (500 MHz, $CDCl_3$) δ 7.16 (dd, J = 5.2, 3.1 Hz, 1H), 6.77 (dd, J = 5.3, 1.6 Hz, 1H), 6.26 (dd, J = 3.2, 1.6 Hz, 1H), 4.15−4.08 (m, 2H), 3.87−3.81 (m, 2H), 3.75 (t, J = 6.5 Hz, 2H), 3.72−3.56 (m, 10H), 2.59 (t, J = 6.5 Hz, 2H)). (^{13}C NMR (126 MHz, $CDCl_3$) δ 172.2, 157.8, 124.9, 124.8, 119.8, 119.8, 97.7, 77.5, 77.2, 77.0, 71.0, 70.9, 70.8, 70.7, 70.6, 69.9, 69.9, 69.8, 66.8, 51.8, 35.1, 35.1.)

Compound C: Methyl 4-(2-(2-(2-((2,5-dibromothiophen-3-yl)oxy)ethoxy)ethoxy)ethoxy)propanoate. *Bromination.* In a typical procedure, compound 2 (0.5072 g, 1.41 mmol, 1 equiv) was dissolved in 10 mL of tetrahydrofuran in a two-neck 50 mL round-bottom flask and purged with N_2 for 30 min. The solution was cooled to 0 °C for 15 min before N-bromo succinimide (0.50 g, 2.82 mmol, 2 equiv) was added portion wise. The mixture was reacted for 1.5 h at 0 °C, an additional small portion of N-bromo succinimide (0.06 mg, 0.32 mmol, 0.2 equiv) was added after 5 h to drive the reaction to completion, after which the reaction was allowed to warm to room temperature and react overnight. The reaction was neutralized by stirring with sodium bicarbonate (5 mL, 1 M) for 15 min. The solution was transferred to an extraction flask along with 40 mL of diethyl ether. The organic phase was extracted with 1 × 50 mL of 1 M sodium bicarbonate and 3 × 50 mL of brine. The water phase was extracted with 2 × 50 mL of diethyl ether. The organic phases were combined and dried over sodium sulfate and magnesium sulfate. The solvent was removed by evaporation, and the product was dried in vacuo overnight. The product was purified on a silica gel column and eluted with 80:20 petroleum ether:acetone. The final yield was 0.35 g (45%) of pure product collected as a yellow oil. The ^{1}H NMR is depicted in in Figures S5 and S6 respectively. (^{1}H NMR (500 MHz, CDCl3) δ 6.85 (s, 1H), 4.19 (dd, J = 5.7, 4.1 Hz, 2H), 3.90−3.83 (m, 2H), 3.78−3.70 (m, 4H), 3.70−3.59 (m, 9H), 2.60 (t, J = 6.5 Hz, 2H)). (^{13}C NMR (126 MHz, CDCl3) δ 172.04, 153.76, 121.51, 109.60, 91.38, 77.28, 77.02, 76.77, 72.06, 71.01, 70.69, 70.58, 70.46, 69.84, 66.61, 51.68, 34.89.)

Compound D: PCAT-Me. *Stille Coupling.* A dry 50 mL two-neck round-bottom flask was charged with compound 3 (0.3 g, 0.63 mmol), 2,5- bis(trimethylstannyl)thiophene (0.297 g, 0.63 mmol, 1.0 equiv), tris(dibenzylideneacetone)-dipalladium(0) (12 mg, 2 mol %), P(o-tolyl)$_3$phosphine (15.3 mg, 8 mol %) and dissolved in dry, purged tetrahydrofuran (10 mL). The solution was heated to 55 °C while stirring, during which the color progressed to deep red and the viscosity increased. After 52 h reaction time, the solution was cooled to room temperature and precipitated in petroleum ether under vigorous stirring which yielded blue fibrous particles. The polymer was collected via centrifugation (3600 rpm for 20 min) before being redissolved in chloroform and vigorously stirred with sodium diethyldithiocarbamate trihydrate (5% m/v, 0.43 g in 0.5 mL water) at 50 °C for 1 h under N_2 to remove palladium. After liquid−liquid extraction, the chloroform solution was reduced in volume, precipitated in petroleum ether and transferred to a Soxhlet extraction thimble. The polymer was Soxhlet extracted with petroleum ether followed by isopropanol until each washing yielded a clear extract. After collection in chloroform and drying the polymer solution *in vacuo*, the polymer was precipitated in petroleum ether, dried under vacuum to yield 290 mg (80%) of the target material as a dark purple sticky solid. ^{1}H NMR is depicted in Figure S7. (^{1}H NMR (500 MHz, $CDCl_3$) δ 7.07 (d, 2H), 6.97 (s, 1H), 4.33 (s, 2H), 4.00 − 3.17 (m, 17H), 2.59 (dt, 3H)).

Compound E: PCAT-K. *Base-Catalyzed Deprotection and Formation of the Polyanion.* A dry 50 mL two-necked round-bottom flask was loaded with 73 mg of compound 4 and 10 mL of sparged THF. 20 mL of sparged 10 w% KOH was added, and the mixture was heated to 55 °C overnight. The polymer was precipitated in N_2 sparged isopropanol (45 mL) and collected via centrifugation. The pellet washed with diethyl ether (45 mL) followed by acetone (45 mL) before drying *in vacuo* to yield 72 mg of polymer as a dark solid.

^{1}H NMR indicated that the deprotection was successful but could not supply in-depth structural characterization due to severe line broadening (see Figure S8).

Batch Variations PCAT Synthesis

The previously reported synthetic protocol[26] for PCAT-K, via PCAT-*t*Bu and deprotected with trifluoracetic acid (TFA, see Scheme S1 and Figure S28), was shown to give variations in final polymer water solubility when repeated by different chemists (Table S1). This was linked to the unwanted formation of chemical cross-links during the workup stage due to the presence of acid and oxygen. To avoid the use of the acidic halogenated deprotecting agent TFA, the synthetic route reported in this article was developed. Solubility of the final polymer was investigated by adding PCAT-K to DI water, and visually inspecting whether any particles were left after 20 min at 50 °C.

Characterization Techniques

Nuclear Magnetic Resonance (NMR). NMR spectra were recorded at room temperature on a Bruker 500 spectrometer (^{1}H: 500 MHz and ^{13}C: 150 MHz) using Topspin software. The ^{1}H and ^{13}C NMR spectra were referenced to the residual proton signal of the deuterated solvent ($CDCl_3$: $\delta(^1H)$ = 7.26 ppm, $\delta(^{13}C)$ = 77.16 ppm, D_2O: $\delta(^1H)$ = 4.79 ppm).

Size-Exclusion Chromatography (SEC). SEC was performed on an Agilent 1280 Infinity system with 2 columns and precolumn (Polargel M 300 × 7.5 mm, 8 μm pore size, mixed pores) fitted with refractive index and viscometry detectors. The eluent was 1 w% LiBr in DMF at 70 °C, calibration curves were obtained from Agilent EasyVial PMMA standards, and all data analysis was performed in the Agilent GPC software. Samples were prepared by dissolving 1 mg mL^{-1} of the sample in DMF by stirring at 80 °C overnight in the dark. The samples were filtered through 0.2 μm disk filters before analysis.

Titration for p*Ka* Determination. Titration for p*Ka* determination was performed on a Metrohm autotitrator equipped with pH and conductivity sensors. Around 30 mg of sample was dissolved in 60 mL of water and titrated with 0.01 M HCl with 0.05 mL additions. Results were recorded in OMNIS software.

ATR-FTIR. ATR-FTIR was performed on a Bruker Equinox mid-IR spectrometer with a DTGS detector, using a diamond-ATR setup. The samples were analyzed in solid or liquid form at wavelengths between 370 and 4000 reciprocal centimeters.

Thin film samples for ATR-FTIR were prepared by the following protocols:

- PCAT-*t*Bu: A 20 mg mL^{-1} chloroform solution of PCAT-*t*Bu was dropcast on gold-plated glass and dried carefully on a hot plate. Acid fixation was done to prove that it does not affect the side chain by dipping the sample in 20 mg mL^{-1} citric acid in isopropanol. Doping was done by soaking the films in 250 mg mL^{-1} *p*-toluenesulfonic acid (*p*-TsOH) overnight.

- PCAT-K: A 20 mg mL^{-1} water solution of PCAT-K was drop-casted on 100 nm gold-plated glass, dried carefully on a hot plate and the polymer was acid fixated by 10 min dip in 10 mg mL^{-1} citric acid in isopropanol. Doping was performed by placing drops of 100 mg mL^{-1} *p*-TsOH on the sample and leaving the samples with airflow overnight in the dark. Doping in the presence of KI was performed by placing drops of 100 mg mL^{-1} *p*-TsOH and 50 mg mL^{-1} KI on the sample and doping for 2 h in air.

UV−vis-NIR Spectroscopy. UV−vis-NIR spectra were recorded using an AvaSpec-NIR256−2.5-HSC-EVO fiber optic spectrophotometer using deuterium (78 W/0,75 A for 190−400 nm) and halogen (5 W/0,5 A, 360−2500 nm) lamps. When studying polymer interaction with hydrogen peroxide, a halogen lamp (360−2500 nm range) was used as the light source to avoid excitation of H_2O_2 in the UV region.

Samples for UV−vis-NIR were prepared by the following protocols:

https://doi.org/10.1021/acs.chemmater.6c01062
Chem. Mater. XXXX, XXX, XXX−XXX

- A stock solution of PCAT-*t*Bu (1 mg mL^{-1}) was prepared with chloroform and diluted to a 0.3 mg mL^{-1} sample that was analyzed in a quartz cuvette.
- A stock solution of PCAT-K (10 mg mL^{-1}) was prepared with water and diluted to a 0.1 mg mL^{-1} sample that was analyzed in a quartz cuvette.
- Samples in solid state were analyzed by spin-coating or drop-casting the polymer on cleaned glass slides (2.3 × 2.3 cm), performing the desired fixation or doping, drying the sample and analyzing it by letting the beam pass through the sample.
- Glass slides were cleaned by 10 min sonication in a soapy water bath, followed by rinsing with DI water, acetone and isopropanol before drying with pressurized air.

Electron Paramagnetic Resonance (EPR). EPR was carried out using a Spinscan X Benchtop EPR equipped with an X-band operating frequency. Capillaries with a 50 μL capacity were used as solution sample holders.

Rutherford Backscattering (RBS) and Particle induced X-ray emission (PIXE). RBS and PIXE were performed on PCAT-K drop-casted on carbon cloth using a primary beam of 2 MeV $^4He^+$ ions provided by the 5MV pelletron tandem accelerator at Uppsala University [10.1088/1748−0221/17/04/P04011]. Backscattered ions were detected under a scattering angle of 170°. Analysis of RBS spectra was performed using the SIMNRA simulation package.[57] PIXE spectra were recorded using a silicon drift detector.

Inductively Coupled Plasma Mass Spectrometry (ICP-MS). ICP-MS for elemental analysis of Pd, Fe and Cu was performed by Mikroanalytisches Laboratorium Kolbe in Germany (www.mikro-lab.de).

Small Angle X-ray Scattering (SAXS). SAXS measurements were performed at the I22 beamline at Diamond Light Source (UK). The beamline was operated at an energy of 12.4 keV and the sample-to-detector distance was set to 1.973 m to cover an angular range of $0.092 \leq q \leq 8.7$ nm^{-1}. Samples were loaded in a quartz capillary of 2 mm in diameter and assembled on a capillary holder. For each sample, 10 frames of 100 ms were collected and averaged.

The raw data was processed using the Dawn Science software (version 2.27)[58] according to a standard I22 pipeline[59] to give 1D plots. The scattering from the H_2O background was subtracted from the PCAT-K solutions using Primus, resulting in the I vs q plots.

The form factor amplitude ($P(q)$) of a cylinder with spherical cross section can be expressed as

$$P(q) = \int_0^{\pi/2} \left[\frac{2J_1(qR\sin\alpha)}{qR\sin\alpha} \frac{\sin(qL\cos\alpha/2)}{qL\cos\alpha/2} \right]^2 \sin\alpha \mathrm{d}\alpha$$

where J_1 is the first order Bessel function of the first kind, R is the radius of the cross section and L is the length of the cylinder. Describing the slight aggregation in case of 6 mg mL^{-1} sample a power law function was also included. Thus, the final equation reads as

$$I(q) = \frac{N}{V}\Delta\rho^2 V_p^2 P_{cyl}(q) + \text{scale} \times q^{-d}$$

where $\frac{N}{V}$ is the number concentration of the particles, $\Delta\rho$ is the excess scattering length density, V_p is the volume of scattering particles, *scale* is the scaling factor of power law function and d is the exponent.

Data modeling was performed using SasView 5.0.4 (http://www.sasview.org/).

Cyclic Voltammetry (CV). CV was performed in acetonitrile solution with 0.2 M tetrabutylammonium hexafluorophosphate ($TBAPF_6$) electrolyte, using a gold PCAT-K-coated electrode as working electrode, a Pt-mesh as counter electrode and Ag/AgCl as the reference electrode (See Figure S29).

Scanning Electron Microscopy (SEM). SEM was performed on Zeiss Sigma 500 scanning electron microscope using InLens detector (acceleration voltage 3 keV). Samples were prepared in the same way as a doping test on threads. Thread samples were mounted with copper tape in horizontal sample holders. Cross section samples were prepared by mounting threads with copper tape on a vertical support and cutting with a scalpel in line with the edge of the support.

Energy-Dispersive X-ray Analysis (EDX). EDX was performed on Zeiss Sigma 500 scanning electron microscope fitted with a Bruker X-ray detector. Samples were prepared in the same way as doping studies on threads, mounted with copper tape and analyzed at an acceleration voltage of 5 keV.

■ ASSOCIATED CONTENT

Data Availability Statement

The data supporting this article has been included as part of the Supporting Information.

Supporting Information

The Supporting Information is available free of charge at https://pubs.acs.org/doi/10.1021/acs.chemmater.6c01062.

Additional details on experimental procedures, as well as supplementary tables and characterization data from NMR, UV−vis−NIR, FTIR, RBS, PIXE, ICP-MS, DLS, EPR, EDX, XRD, and cyclic voltammetry analyses (PDF)

■ AUTHOR INFORMATION

Corresponding Authors

Johanna Heimonen − *Laboratory of Organic Electronics, Department of Science and Technology, Linköping University, Norrköping SE-601 74, Sweden; Wallenberg Wood Science Center, Linköping University, Norrköping SE-601 74, Sweden*; Email: johanna.heimonen@liu.se

Renee Kroon − *Laboratory of Organic Electronics, Department of Science and Technology, Linköping University, Norrköping SE-601 74, Sweden; Wallenberg Wood Science Center and Wallenberg Initiative Materials Science for Sustainability, Linköping University, Norrköping SE-601 74, Sweden*; orcid.org/0000-0001-8053-4288; Email: renee.kroon@liu.se

Authors

Cecilia Bruschi − *Laboratory of Organic Electronics, Department of Science and Technology, Linköping University, Norrköping SE-601 74, Sweden; Wallenberg Initiative Materials Science for Sustainability, Linköping University, Norrköping SE-601 74, Sweden*

Asaminew Y. Shimolo − *Laboratory of Organic Electronics, Department of Science and Technology, Linköping University, Norrköping SE-601 74, Sweden; Wallenberg Wood Science Center, Linköping University, Norrköping SE-601 74, Sweden*

Marle E. J. Vleugels − *Laboratory of Organic Electronics, Department of Science and Technology, Linköping University, Norrköping SE-601 74, Sweden*

Lukas Marcos Celada − *Laboratory of Organic Electronics, Department of Science and Technology, Linköping University, Norrköping SE-601 74, Sweden; Wallenberg Wood Science Center, Linköping University, Norrköping SE-601 74, Sweden; Division of Biocomposites, Department of Fiber and Polymer Technology, KTH Royal Institute of Technology, 100 44 Stockholm, Sweden*

Sozan Darabi − *Department of Chemistry and Chemical Engineering and Wallenberg Wood Science Center, Chalmers University of Technology, Göteborg 41296, Sweden*

Viktor Gueskine − *Laboratory of Organic Electronics, Department of Science and Technology, Linköping University, Norrköping SE-601 74, Sweden*

Daniel Primetzhofer − *Department of Physics and Astronomy Materials Physics, Uppsala University, 75137 Uppsala, Sweden;* orcid.org/0000-0002-5815-3742

Christian Müller − *Department of Chemistry and Chemical Engineering and Wallenberg Wood Science Center, Chalmers University of Technology, Göteborg 41296, Sweden;* orcid.org/0000-0001-7859-7909

Bence Fehér − *Nanobiophysics Research Group, HUN-REN Office for Supported Research Groups, Institute of Biophysics and Radiation Biology, Semmelweis University, 1094 Budapest, Hungary*

Peter Olsén − *Laboratory of Organic Electronics, Department of Science and Technology, Linköping University, Norrköping SE-601 74, Sweden; Wallenberg Wood Science Center, Linköping University, Norrköping SE-601 74, Sweden;* orcid.org/0000-0002-5081-1835

Complete contact information is available at: https://pubs.acs.org/10.1021/acs.chemmater.6c01062

Author Contributions

J.H., R.K., and C.M. conceived the study. J.H. performed the initial synthesis, developed the coating and doping protocols for thin films and threads, and performed the analysis related to these. C.B. performed the hydrogen peroxide and radical measurements and formulated the suggested mechanism together with R.K. A.Y.S. developed the optimized synthetic route with help from J.H. M.E.J.V. provided beamtime and SAXS data analysis. L.M.C performed XRD measurements and interpretation. SD performed initial testing of PCAT-coated threads. V.G provided essential insight into the hydrogen peroxide formation mechanisms. D.P. performed RBS and PIXE analysis and interpretation. B.F. performed the fitting of SAXS data and interpretation of the results. P.O. and RK. supervised the study. J.H., C.B., M.E.J.V., and R.K. prepared the manuscript, with help from the coauthors.

Notes

The authors declare no competing financial interest.

■ ACKNOWLEDGMENTS

R.K. and C.B. acknowledge funding from the Wallenberg Initiative Material Science for Sustainability (WISE) and the Swedish Research Council (2024-05023). R.K., A.Y.S, S.D., C.M. and J.H. acknowledge the Knut and Alice Wallenberg Foundation (KAW) through the Wallenberg Wood Science Center (2021.0313) and through the project "Stable Doping of Organic Semiconductors" (2022.0034). C.B. acknowledges MATTER Call for Innovative Research Projects 2025. The authors would like to thank the Diamond Light Source, UK, for the award of X-ray beamtime (proposal SM39422), and to the staff on beamline I22 for their assistance with the synchrotron X-ray experiments. Accelerator operation at Uppsala University was supported by the Swedish research Council VR-RFI (2019-00191). The authors would also like to thank Lars Gustavsson, Thomas Karlsson and Peter Holmberg, without whose efforts, most of this work would not have been possible.

■ REFERENCES

(1) Anastas, P. T.; Zimmerman, J. B. The periodic table of the elements of green and sustainable chemistry. *Green Chem.* **2019**, *21* (24), 6545−6566.

(2) European Commission: Directorate-General for, R.; Innovation. *Safe and Sustainable by Design Chemicals and Materials − A European Assessment Framework*, Publications Office of the European Union, 2022.

(3) McQuade, D. T.; Pullen, A. E.; Swager, T. M. Conjugated polymer-based chemical sensors. *Chem. Rev.* **2000**, *100* (7), 2537−2574.

(4) Jang, J. Conducting polymer nanomaterials and their applications. *Emissive Materials Nanomaterials*; Springer, 2006189−260.

(5) Palani, P.; Karpagam, S. Conjugated polymers−a versatile platform for various photophysical, electrochemical and biomedical applications: a comprehensive review. *New J. Chem.* **2021**, *45* (41), 19182−19209.

(6) Fan, X.; Stott, N. E.; Zeng, J.; Li, Y.; Ouyang, J.; Chu, L.; Song, W. PEDOT: PSS materials for optoelectronics, thermoelectrics, and flexible and stretchable electronics. *J. Mater. Chem. A* **2023**, *11* (35), 18561−18591.

(7) Nilsson, D.; Kugler, T.; Svensson, P.-O.; Berggren, M. An all-organic sensor−transistor based on a novel electrochemical transducer concept printed electrochemical sensors on paper. *Sens. Actuators, B* **2002**, *86* (2−3), 193−197.

(8) Grimsdale, A.; Dastoor, P. *Conjugated Polymers for Organic Electronics: Design and Synthesis*; Cambridge University Press, 2024.

(9) Brooke, R.; Lay, M.; Jain, K.; Francon, H.; Say, M. G.; Belaineh, D.; Wang, X.; Håkansson, K. M. O.; Wågberg, L.; Engquist, I.; et al. Nanocellulose and PEDOT:PSS composites and their applications. *Polym. Rev.* **2023**, *63* (2), 437−477.

(10) Tran, V. C.; Mastantuoni, G.; Garemark, J.; Dreimol, C. H.; Wang, X.; Berggren, M.; Zhou, Q.; Kroon, R.; Engquist, I. Interconnecting EDOT-Based Polymers with Native Lignin toward Enhanced Charge Storage in Conductive Wood. *ACS Appl. Mater. Interfaces* **2024**, *16* (49), 68416−68425.

(11) Darabi, S.; Hummel, M.; Rantasalo, S.; Rissanen, M.; Öberg Månsson, I.; Hilke, H.; Hwang, B.; Skrifvars, M.; Hamedi, M. M.; Sixta, H.; et al. Green Conducting Cellulose Yarns for Machine-Sewn Electronic Textiles. *ACS Appl. Mater. Interfaces* **2020**, *12* (50), 56403−56412.

(12) Mone, M.; Kim, Y.; Darabi, S.; Zokaei, S.; Karlsson, L.; Craighero, M.; Fabiano, S.; Kroon, R.; Müller, C. Mechanically Adaptive Mixed Ionic-Electronic Conductors Based on a Polar Polythiophene Reinforced with Cellulose Nanofibrils. *ACS Appl. Mater. Interfaces* **2023**, *15* (23), 28300−28309.

(13) García-Valverde, R.; Cherni, J. A.; Urbina, A. Life cycle analysis of organic photovoltaic technologies. *Prog. Photovoltaics Res. Appl.* **2010**, *18* (7), 535−558.

(14) Uva, A.; Michailovich, S.; Hsu, N. S. Y.; Tran, H. Degradable π-Conjugated Polymers. *J. Am. Chem. Soc.* **2024**, *146* (18), 12271−12287.

(15) Lei, T.; Guan, M.; Liu, J.; Lin, H.-C.; Pfattner, R.; Shaw, L.; McGuire, A. F.; Huang, T.-C.; Shao, L.; Cheng, K.-T.; et al. Biocompatible and totally disintegrable semiconducting polymer for ultrathin and ultralightweight transient electronics. *Proc. Natl. Acad. Sci. U.S.A.* **2017**, *114* (20), 5107−5112.

(16) Tran, H.; Feig, V. R.; Liu, K.; Wu, H.-C.; Chen, R.; Xu, J.; Deisseroth, K.; Bao, Z. Stretchable and Fully Degradable Semiconductors for Transient Electronics. *ACS Cent. Sci.* **2019**, *5* (11), 1884−1891.

(17) Chen, J.; Cong, S.; Liu, R.; Duan, J.; Chen, C.; Yu, D.; Zhu, X.; Ran, C.; Cheng, D.; Li, Z.; et al. Imine-Based Polymeric Mixed Ionic−Electronic Conductors Featuring Degradability and Biocompatibility for Transient Bioinspired Electronics. *Angew. Chem., Int. Ed.* **2025**, *64* (10), No. e202417921.

(18) Jin, H.; Kim, K.; Park, S.; Rhee, J.; Ahn, H.; Kim, D. J.; Kim, K.; Noh, J. H.; Kim, T.-S.; Shin, E.-Y.; Son, H. J. Chemically Recyclable Conjugated Polymer and One-Shot Preparation of Thermally Stable and Efficient Bulk-Heterojunction from Recycled Monomer. *Adv. Funct. Mater.* **2023**, *33* (47), No. 2304930.

(19) Tian, S.; Yue, Q.; Liu, C.; Li, M.; Yin, M.; Gao, Y.; Meng, F.; Tang, B. Z.; Luo, L. Complete Degradation of a Conjugated Polymer into Green Upcycling Products by Sunlight in Air. *J. Am. Chem. Soc.* **2021**, *143* (27), 10054−10058.
(20) Huang, H.; Xie, W.; Wan, Q.; Mao, L.; Hu, D.; Sun, H.; Zhang, X.; Wei, Y. A Self-Degradable Conjugated Polymer for Photodynamic Therapy with Reliable Postoperative Safety. *Adv. Sci.* **2022**, *9* (4), No. 2104101.
(21) Stavrinidou, E.; Leleux, P.; Rajaona, H.; Khodagholy, D.; Rivnay, J.; Lindau, M.; Sanaur, S.; Malliaras, G. G. Direct Measurement of Ion Mobility in a Conducting Polymer. *Adv. Mater.* **2013**, *25* (32), 4488−4493.
(22) Khau, B. V.; Savagian, L. R.; De Keersmaecker, M.; Gonzalez, M. A.; Reichmanis, E. Carboxylic Acid Functionalization Yields Solvent-Resistant Organic Electrochemical Transistors. *ACS Mater. Lett.* **2019**, *1* (6), 599−605.
(23) Sun, Z.; Khau, B.; Dong, H.; Takacs, C. J.; Yuan, S.; Sun, M.; Lis, B. M.; Nguyen, D.; Reichmanis, E. Carboxyl-Alkyl Functionalized Conjugated Polyelectrolytes for High Performance Organic Electrochemical Transistors. *Chem. Mater.* **2023**, *35* (21), 9299−9312.
(24) Sun, Z.; Sun, M.; Qin, S.; Wang, M.; Zheng, Y.; Khau, B.; Li, H.; Gartner III, T. E.; Takacs, C. J.; Reichmanis, E. Controlling Ion Uptake in Carboxylated Mixed Conductors. *Adv. Mater.* **2025**, *37* (8), No. 2414963.
(25) Hofmann, A. I.; Kroon, R.; Yu, L.; Müller, C. Highly stable doping of a polar polythiophene through co-processing with sulfonic acids and bistriflimide. *J. Mater. Chem. C* **2018**, *6* (26), 6905−6910.
(26) Liu, T.; Heimonen, J.; Zhang, Q.; Yang, C.-Y.; Huang, J.-D.; Wu, H.-Y.; Stoeckel, M.-A.; van der Pol, T. P. A.; Li, Y.; Jeong, S. Y.; et al. Ground-state electron transfer in all-polymer donor:acceptor blends enables aqueous processing of water-insoluble conjugated polymers. *Nat. Commun.* **2023**, *14* (1), No. 8454.
(27) Facchetti, A. π-Conjugated polymers for organic electronics and photovoltaic cell applications. *Chem. Mater.* **2011**, *23* (3), 733−758.
(28) Rivnay, J.; Inal, S.; Salleo, A.; Owens, R. M.; Berggren, M.; Malliaras, G. G. Organic electrochemical transistors. *Nat. Rev. Mater.* **2018**, *3* (2), 1−14.
(29) Han, C.; Elsenbaumer, R. Protonic acids: Generally applicable dopants for conducting polymers. *Synth. Met.* **1989**, *30* (1), 123−131.
(30) Jarvis, M. C. Hydrogen bonding and other non-covalent interactions at the surfaces of cellulose microfibrils. *Cellulose* **2023**, *30* (2), 667−687.
(31) Zou, S.; Lv, R.; Tong, Z.; Na, B.; Fu, K.; Liu, H. In situ hydrogen-bonding complex mediated shape memory behavior of PAA/PEO blends. *Polymer* **2019**, *183*, No. 121878.
(32) Nadeau, F.; Sindt, M.; Oget, N. Free-solvent Michael addition of glycerol to acrylic compounds. *New J. Chem.* **2015**, *39* (12), 9155−9161.
(33) Li, Y.; Li, H.; Chen, X.; Zhu, F.; Yang, J.; Zhu, Y. Complexation of poly(acrylic acid) and poly(ethylene oxide) investigated by enhanced Rayleigh scattering method. *J. Polym. Sci., Part B: Polym. Phys.* **2010**, *48* (16), 1847−1852.
(34) Mammone, R. J.; MacDiarmid, A. G. p-Doping of (CH) to the metallic regime with gaseous oxygen. Application to oxygen fuel-cell-type electrodes. *J. Chem. Soc., Faraday Trans. 1* **1985**, *81* (1), 105−112.
(35) Cendra, C.; Giovannitti, A.; Savva, A.; Venkatraman, V.; McCulloch, I.; Salleo, A.; Inal, S.; Rivnay, J. Role of the Anion on the Transport and Structure of Organic Mixed Conductors. *Adv. Funct. Mater.* **2019**, *29* (5), No. 1807034.
(36) Gueskine, V.; Singh, A.; Vagin, M.; Crispin, X.; Zozoulenko, I. Molecular Oxygen Activation at a Conducting Polymer: Electrochemical Oxygen Reduction Reaction at PEDOT Revisited, a Theoretical Study. *J. Phys. Chem. C* **2020**, *124* (24), 13263−13272.
(37) Gueskine, V.; Vagin, M.; Berggren, M.; Crispin, X.; Zozoulenko, I. Oxygen reduction reaction at conducting polymer electrodes in a wider context: Insights from modelling concerning outer and inner sphere mechanisms. *Electrochem. Sci. Adv.* **2023**, *3* (2), No. e2100191.
(38) De La Fuente Durán, A.; Liang, A. Y.-L.; Denti, I.; Yu, H.; Pearce, D.; Marks, A.; Penn, E.; Treiber, J.; Weaver, K.; Turaski, L.; et al. Origins of hydrogen peroxide selectivity during oxygen reduction on organic mixed ionic−electronic conducting polymers. *Energy Environ. Sci.* **2023**, *16* (11), 5409−5422.
(39) Luo, Y.-R. *Comprehensive Handbook of Chemical Bond Energies*; CRC press, 2007.
(40) Fenton, H. J. H. LXXIII.—Oxidation of tartaric acid in presence of iron. *J. Chem. Soc., Trans.* **1894**, *65*, 899−910.
(41) Haber, F.; Weiss, J. The catalytic decomposition of hydrogen peroxide by iron salts. *Proc. R. Soc. London, Ser. A* **1934**, *147* (861), 332−351.
(42) Choi, J. S.; Fortunato, G. V.; Jung, D. C.; Lourenço, J. C.; Lanza, M. R.; Ledendecker, M. Catalyst durability in electrocatalytic H 2 O 2 production: key factors and challenges. *Nanoscale Horiz.* **2024**, *9* (8), 1250−1261.
(43) Liu, T. Z.; Lin, T. F.; Chiu, D. T. Y.; Tsai, K.-J.; Stern, A. Palladium or Platinum Exacerbates Hydroxyl Radical Mediated DNA Damage. *Free Radical Biol. Med.* **1997**, *23* (1), 155−161.
(44) Chausson, M.; Fluchère, A.-S.; Landreau, E.; Aguni, Y.; Chevalier, Y.; Hamaide, T.; Abdul-Malak, N.; Bonnet, I. Block copolymers of the type poly(caprolactone)-b-poly(ethylene oxide) for the preparation and stabilization of nanoemulsions. *Int. J. Pharm.* **2008**, *362* (1), 153−162.
(45) Liao, H.-H.; Yang, C.-M.; Liu, C.-C.; Horng, S.-F.; Meng, H.-F.; Shy, J.-T. Dynamics and reversibility of oxygen doping and de-doping for conjugated polymer. *J. Appl. Phys.* **2008**, *103* (10), No. 104506.
(46) Payá, M.; Halliwell, B.; Hoult, J. Interactions of a series of coumarins with reactive oxygen species: scavenging of superoxide, hypochlorous acid and hydroxyl radicals. *Biochem. Pharmacol.* **1992**, *44* (2), 205−214.
(47) Louit, G.; Foley, S.; Cabillic, J.; Coffigny, H.; Taran, F.; Valleix, A.; Renault, J. P.; Pin, S. The reaction of coumarin with the OH radical revisited: hydroxylation product analysis determined by fluorescence and chromatography. *Radiat. Phys. Chem.* **2005**, *72* (2−3), 119−124.
(48) Cook, M. K.; Dial, A. R.; Hendy, I. L. Iodine stability as a function of pH and its implications for simultaneous multi-element ICP-MS analysis of marine carbonates for paleoenvironmental reconstructions. *Mar. Chem.* **2022**, *245*, No. 104148.
(49) Goto, H. A Possibility for Construction of an Iodine Cleaning System Based on Doping for π-Conjugated Polymers. *Polymers* **2011**, *3* (2), 875−885.
(50) Lund, A.; van der Velden, N. M.; Persson, N.-K.; Hamedi, M. M.; Müller, C. Electrically conducting fibres for e-textiles: An open playground for conjugated polymers and carbon nanomaterials. *Mater. Sci. Eng., R* **2018**, *126*, 1−29.
(51) Alshabouna, F.; Lee, H. S.; Barandun, G.; Tan, E.; Cotur, Y.; Asfour, T.; Gonzalez-Macia, L.; Coatsworth, P.; Núnez-Bajo, E.; Kim, J.-S.; Güder, F. PEDOT:PSS-modified cotton conductive thread for mass manufacturing of textile-based electrical wearable sensors by computerized embroidery. *Mater. Today* **2022**, *59*, 56−67.
(52) Darabi, S.; Yang, C.-Y.; Li, Z.; Huang, J.-D.; Hummel, M.; Sixta, H.; Fabiano, S.; Müller, C. Polymer-Based n-Type Yarn for Organic Thermoelectric Textiles. *Adv. Electron. Mater.* **2023**, *9* (4), No. 2201235.
(53) Lv, J.; Dai, Y.; Xu, H.; Zhong, Y.; Zhang, L.; Chen, Z.; Sui, X.; Feng, X.; Wang, B.; Mao, Z. Transforming commercial regenerated cellulose yarns into multifunctional wearable electronic textiles. *J. Mater. Chem. C* **2020**, *8* (4), 1309−1318.
(54) Carrillo, F.; Colom, X.; Suñol, J. J.; Saurina, J. Structural FTIR analysis and thermal characterisation of lyocell and viscose-type fibres. *Eur. Polym. J.* **2004**, *40* (9), 2229−2234.
(55) Alarcon-Espejo, P.; Sarabia-Riquelme, R.; Matrone, G. M.; Shahi, M.; Mahmoudi, S.; Rupasinghe, G. S.; Le, V. N.; Mantica, A. M.; Qian, D.; Balk, T. J.; et al. High-Hole-Mobility Fiber Organic Electrochemical Transistors for Next-Generation Adaptive Neuromorphic Bio-Hybrid Technologies. *Adv. Mater.* **2024**, *36* (11), No. 2305371.

(56) Tashiro, K.; Gakhutishvili, M. Crystal structure of cellulose-iodine complex. *Polymer* **2019**, *171*, 140−148.
(57) Mayer, M.; Guide, S. U. *Technical Report IPP 9/113* Max-Planck-Institut für Plasmaphysik: Garching, Germany; 1997.
(58) Filik, J.; Ashton, A. W.; Chang, P. C. Y.; Chater, P.; Day, S.; Drakopoulos, M.; Gerring, M.; Hart, M.; Magdysyuk, O.; Michalik, S.; et al. Processing two-dimensional X-ray diffraction and small-angle scattering data in DAWN 2. *App. Crystallogr.* **2017**, *50* (3), 959−966.
(59) Pauw, B. R.; Smith, A. J.; Snow, T.; Terrill, N. J.; Thünemann, A. F. The modular SAXS data correction sequence for solids and dispersions. 2017, arXiv:1706.06769. arXiv.org e-Print archive. https://arxiv.org/abs/1706.06769.

https://doi.org/10.1021/acs.chemmater.6c01062
Chem. Mater. XXXX, XXX, XXX−XXX